JOURNAL OF GUIDANCE, CONTROL, AND DYNAMICS
Vol. 15, No. 2, March-April 1992

Design, Manufacture, and Application to Space Robotics of Distributed Piezoelectric Film Sensors

S. A. Collins,* C. E. Padilla,* R. J. Notestine,† and A. H. von Flotow‡
Massachusetts Institute of Technology, Cambridge, Massachusetts 02139
and
E. Schmitz§ and M. Ramey¶
Martin Marietta Space Systems, Denver, Colorado 80201

This paper describes the development and manufacture of distributed piezoelectric film strain sensors. The sensors are spatially shaped such that, when bonded to a vibrating structure, their output is selectively proportional to a particular deformation pattern of the flexible structure. In this paper, the selectivity is based on the spatial orthogonality of the structure's natural modes of vibration, but orthogonality of arbitrary basis functions might also be exploited. The generalized amplitudes of these basis functions are states in a multiple-flexible-body dynamic simulation; the new sensors permit direct measurement of states otherwise available only from a dynamic estimation procedure. An experimental two-link planar manipulator is employed in this study to quantify the performance of these sensors in a dynamic environment. Sensor outputs are compared with the state estimates generated by open-loop simulation and by several Kalman filters. Surprisingly close agreement is found, even for a crude linear estimator. This process can also be viewed as using the piezoelectric film sensors to evaluate state estimation procedures applicable to multiple-flexible-body systems.

Nomenclature

a_h = distance from rotation axis to elastic beam root
a_t = distance from center of mass of payload to tip point of attachment
$b(x)$ = width of polyvinylidene fluoride (PVDF) film's electrode
C_{ki} = gain of sensor k with respect to mode i
D = flexural rigidity of beam
$d_{31}(d_{32})$ = ratio of short-circuit charge per unit electrode area to stress applied along PVDF film's length (width) axis
E_f = Young's modulus of PVDF film
e_{31} = ratio of short-circuit charge per unit electrode area to strain applied along PVDF film's length axis
$H_{col}(s)$ = transfer function from motor torque to motor angular velocity
$H_k(s)$ = transfer function from motor torque to output of modal sensor k
I_{et} = moment of inertia of beam, rotor, and payload about rotation axis
I_h = moment of inertia of rigid elbow rotor about rotation axis
I_t = moment of inertia of payload about tip point of attachment
L = length of elastic beam
m_t = mass of payload
$Q(t)$ = charge developed by PVDF film
$q_i(t)$ = generalized coordinate
$T_e(t)$ = torque applied to elbow joint
$V_k(t)$ = output voltage of sensor k
$w(x,t)$ = transverse displacement of beam
$x(t)$ = state vector
z = distance from beam's neutral axis to midplane of PVDF film
δ_{ij} = Kronecker delta
ζ_i = modal damping coefficient
$\dot{\theta}_E(t)$ = elbow motor angular velocity, $d\theta_E(t)/dt$
ν_b = Poisson's ratio of beam
ν_f = Poisson's ratio of PVDF film
ρ = mass of beam per unit length
$\phi_i(x)$ = eigenfunction
$\phi_i'(0)$ = modal slope $[d\phi_i(x)/dx]$ at root of beam, $x=0$
Ω_i = natural frequency of cantilever beam, rad/s
ω_i = natural frequency of pinned-free beam, rad/s

Introduction

MANY techniques for the control of flexible structures have been developed that use common sensors and complex algorithms to decompose the structure's vibrations into generalized amplitudes of a set of basis functions. The natural modes of vibration of the structural components are often used as basis functions.[1,2] Any control system will be limited by the accuracy and dynamic response of such an estimation approach. Direct measurements of modal amplitudes could serve as inputs to the compensator, thus dispensing with the need for an estimator and theoretically improving the response of the control system.

Miller and Hubbard[3] discussed semidirect measurements of modal amplitude using polyvinylidene fluoride (PVDF) film sensors of general geometry. Recently, Lee and Moon[4] released work in which they investigated sensors shaped proportional to the second derivative of the mode shapes of a cantilever beam. They constructed a small PVDF/shim-stock laminate that included sensors for the first two modes. Good performance was reported for both modal sensors.

Presented as Paper 90-0949 at the AIAA/ASME/ASCE/AHS/ASC 31st Structures, Structural Dynamics, and Materials Conference, Long Beach, CA, April 2-8, 1990; received July 3, 1990; revision received Dec. 7, 1990; accepted for publication Dec. 10, 1990.

*Research Assistant, Space Engineering Research Center, Department of Aeronautics and Astronautics. Student Member AIAA.
†Undergraduate Research Assistant, Space Engineering Research Center, Department of Aeronautics and Astronautics. Student Member AIAA.
‡Associate Professor, Space Engineering Research Center, Department of Aeronautics and Astronautics. Member AIAA.
§Staff Engineer, Robotics Section, Research and Technology Department.
¶Senior Engineer, Robotics Section, Research and Technology Department.

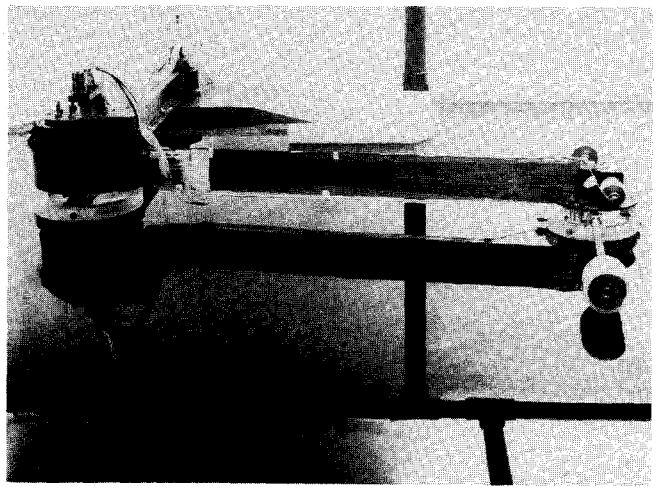

Fig. 1 Martin Marietta two-link planar flexible manipulator.

Notestine and Beninato[5] used modal sensors on a clamped-free steel beam and attempted to measure higher modes. Their work met with partial success, since the first, third, and fourth mode sensors yielded excellent results, whereas the sensor for the second mode suffered from manufacturing-related difficulties. The purpose of the present work is to address those difficulties and to validate the use of modal sensors by demonstrating their effectiveness when applied to a problem of current interest, specifically, the control of lightweight manipulators with distributed flexibility for space applications. With this in mind, modal sensors designed and manufactured at the Massachusetts Institute of Technology (MIT) were studied on a flexible manipulator testbed designed and maintained at Martin Marietta Astronautics.

Modal Sensor Theory

Piezoelectric materials exhibit a coupling between mechanical and electrical properties that has been the subject of much research in the field of distributed actuators and sensors.[3,4,6-8] This coupling can be described simply as follows: when a voltage is applied across the material, the material deforms; conversely, when the material is strained, a charge collects on its surface. If a thin film of PVDF is mounted on the surface of a single-span beam, the relationship between the developed film charge $Q(t)$ and the beam curvature $w''(x,t)$ can be written as[4]

$$Q(t) = -ze_{31}\int_0^L b(x)w''(x,t)\,dx \tag{1}$$

where

$$e_{31} = (d_{31} + \nu_f d_{32})\frac{E_f}{1-\nu_f^2}$$

The transverse displacement can be decomposed into a series of time-dependent generalized coordinates $q_i(t)$ multiplied by the corresponding space-dependent basis functions as in the assumed modes method. If we let the solutions of the eigenvalue problem, i.e., the eigenfunctions $\phi_i(x)$, associated with the single-span beam be the basis functions, then the orthogonality relations[9] provide a way to fashion *modal sensors*. Let

$$w(x,t) = \sum_{i=1}^{n}\phi_i(x)q_i(t) \tag{2}$$

Then, for uniform beams with a variety of boundary conditions,[10] the secondary orthogonality relation yields

$$\int_0^L \phi_i''(x)\phi_j''(x)\,dx = 0, \qquad i \neq j \tag{3}$$

It is apparent from Eqs. (1-3) that, if the width of the piezoelectric film is proportional to the second derivative of the basis function, the charge developed due to deformation of the beam will be proportional to the corresponding generalized coordinate $q_i(t)$. Thus, a sensor can be designed that measures the generalized coordinates of a flexible beam directly. This allows the feedback of "flexible states" without the need for an estimator.

Testbed Description

Figure 1 shows a photograph of the Large Space Manipulator (LSM) testbed at Martin Marietta. This is an experimental testbed for planar two-dimensional articulated elastic structures. It is used for dynamic model validation as well as for demonstrating various control strategies. The manipulator consists of a 1.8-m planar arm with two lightweight aluminum links of rectangular cross section. The elbow and the tip are supported by air pads floating on a flat table so that the links will only bend in the horizontal plane. Arbitrary positions within a given workspace can be reached using two actuators. The shoulder actuator, a PMI Revex series gearmotor, has a 20:1 gear ratio and provides a peak torque of 110 N·m. The elbow drive is a direct drive Inland dc motor capable of a peak torque of 27 N·m.

The manipulator is normally instrumented with three sets of sensors: position and rate sensors at each joint, strain gauges mounted at several locations along the links, and two accelerometers mounted at the tip along two orthogonal directions. An analog electronics rack is used to amplify and filter the sensor signals. Each actuator is driven by a pulse-width modulated (PWM) amplifier with an adjustable internal current feedback loop. Digital control is implemented with an Intel 310 development system using a 386 single-board processor. Two 16-channel analog-to-digital (A/D) converter boards are used as well as one 8-channel digital-to-analog (D/A) converter board. An electronics interface panel is provided from which the user can monitor each of the A/D and D/A channels and apply external inputs to the actuator amplifiers for open-loop testing.

The real-time control software supports joint-space control as well as Cartesian-space control. In the latter case, the manipulator endpoint is commanded to follow a straight line using a fifth-order spline time profile. The commanded joint positions and velocities are obtained from an inverse kinematic model of the two-link rigid arm. To illustrate the computational speed of the real-time software, we note that joint-space control using an eighth-order fixed-gain compensator with two inputs and five outputs may be performed at a sampling period of 3.5 ms. For Cartesian-control, the minimum sampling period is 5.5 ms. In addition to providing real-time control, the Intel 310 workstation also serves as the user interface. The interface features a series of menus from which the user may specify such parameters as digital sampling rate, reference commands, data recording attributes, and input/output (I/O) port configuration. User-supported subroutines may also be used as control laws.

Basis Function Selection and Sensor Design

The particular testbed configuration chosen for the testing of the modal sensors corresponds to the generic planar articulated structure shown in Fig. 2. The inner link is rigid and the outer link is modeled as an elastic structure composed of a rigid rotor, an Euler-Bernoulli elastic beam that bends only in the plane of motion, and a rigid payload. A dynamic model for this structure, complete to first order in generalized elastic coordinates, can be found in Ref. 11. The basis functions for the decomposition of the outer link transverse displacement $w(x,t)$ were taken as the natural mode shapes of the outer link when the inner link is locked, i.e., the eigenfunctions of the beam pinned at one end with root inertia, tip mass, and tip inertia.

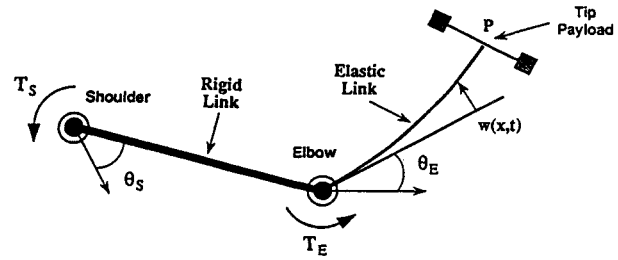

Fig. 2 Schematic of the planar rigid-elastic arm.

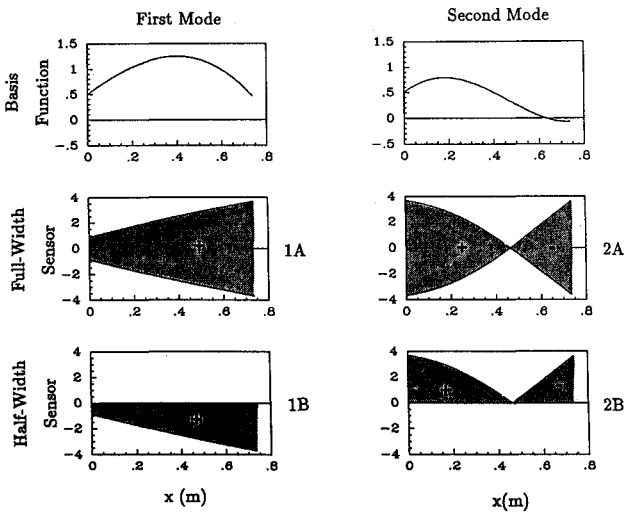

Fig. 3 Assumed basis functions and the corresponding sensor widths (not to scale).

To detect the amplitudes of the first two basis functions, the PVDF sensors were shaped such that their width $b(x)$ was proportional to the second derivatives of these functions. The basis functions were determined analytically using the physical dimensions of the test article given in Table 1. The basis functions and the corresponding sensor shapes are shown in Fig. 3.

The partial differential equation in the unknown $w(x,t)$ for the composite elastic structure (link and endbodies) with the rotation axis fixed in inertial space is

$$D\,\frac{\partial^4 w(x,t)}{\partial x^4} + \rho\,\frac{\partial^2 w(x,t)}{\partial t^2} = 0 \tag{4}$$

with the boundary conditions

$$w(0,t) = a_h w'(0,t)$$

$$I_h \ddot{\theta} = Dw''(0,t) - a_h Dw'''(0,t)$$

$$m_t \ddot{w}(L,t) + m_t a_t \ddot{w}'(L,t) = Dw'''(L,t)$$

$$I_t \ddot{w}'(L,t) + m_t a_t \ddot{w}(L,t) = -Dw''(L,t) \tag{5}$$

Because of the ratio of width to thickness for the link, a one-dimensional plate model[4,12] that accounts for the effects of cylindrical bending is appropriate, i.e., $D = EI/(1-\nu^2)$.

Equation (4) can be solved by the standard method of separation of variables and assumed modes, where the basis functions are chosen to be the natural mode shapes mentioned earlier. The forced vibrations of the pinned-free elastic link can then be described by an infinite set of decoupled modal equations.[9] The basis functions satisfy the following orthogonality relations:

$$\int_E \phi_i(x)\phi_j(x)\,dm = I_{el}\,\delta_{ij} \tag{6}$$

Table 1 Test article properties

Parameter	Value
Beam	0.736 m × 0.076 m × 3.18 mm
I_h	0.0253 kg · m^2
a_h	0.153 m
m_t	4.398 kg
a_t	0.03 m
I_t	0.324 kg · m^2

Table 2 Properties of PVDF film

Parameter	Value
Thickness (total), μm	52
Thickness (electrode), μm	0.1
Piezo strain constant (d_{31}), C/N	23×10^{-12}
Young's modulus, GPa	2.0
Density, kg/m^2	1780
Capacitance, nF	
Sensor 1B	31
Sensor 2A	27
Sensor 2B	56

$$\int_E x\phi_i(x)\,dm = 0 \tag{7}$$

where the integration is done along the composite elastic structure. Equation (7) expresses the orthogonality of the elastic modes to the rigid-body mode $[\phi_0(x) = x]$.

Sensor Manufacture

As suggested in the Introduction, the experimental article under consideration in this paper was the successor of a previous specimen. The film used for the original set of sensors was 52-μm-thick PVDF with silver ink electrodes silk-screened on both sides. Epoxy was used to secure the sensors to a steel cantilever beam; conductive epoxy was used to ground the sensors to the beam. To measure four generalized coordinates, two sensors were layered on each side of the beam, with a piece of fiberglass (250 μm thick) separating the layers of film. Several manufacturing-related problems were encountered during the testing of the first beam. The film did not cut very cleanly, leading to shorting across the thickness due to minute metal shavings. This may have caused the loss of the second mode sensor. The fiberglass was stiffer than the PVDF, resulting in shear loads that affected the output of the third and fourth mode sensors.

The new test article was modified in several ways. Rather than a steel cantilever beam, an aluminum pinned-free beam was used to match the outer link of the experimental manipulator. The film was still 52-μm-thick PVDF, but with vacuum-deposited nickel/copper electrodes rather than silver ink ones; Pennwalt Corporation[13] advertises these as being less susceptible to the risk of shorting. The layering issue was addressed in two ways: half-width sensors and Mylar insulation. On the steel beam, the sensors were symmetric about the beam's centerline and were scaled to be the full width of the beam. One pair of sensors was similarly fashioned for this test article, but a second pair was scaled to be half the width of the beam so that they could be placed side by side. The layered sensors were isolated by a 25-μm-thick layer of Mylar rather than fiberglass. Figure 3 illustrates the difference between the full-width and the half-width sensors. Some details of the piezo film[13] and the sensors are given in Table 2.

The film was cut using templates and a surgical knife. KYNAR piezo film comes in 15 × 30 cm sheets, and so the sensors were made of several segments. As the film is orthotropic and polarized, all pieces were cut lengthwise along the sheets and the upper surface was marked. A sign change in the polarity of the sensors, needed for the second mode sensor, was accomplished by turning the appropriate film seg-

Table 3 Comparison of natural frequencies

Mode no.	Frequency of beam, Hz MIT	MM
1	2.02	2.03
2	9.4	9.93
3	34.8	34.6

ment over. For added experimental flexibility, it was decided not to ground the sensors to the beam, and so the beam was covered with Mylar before the sensors were attached. Other manufacturing techniques for shaped PVDF sensors are presented in Ref. 14.

After the sensors were attached to the beam, sensor 1A (see Fig. 3) appeared to have shorted out, possibly due to the conductive adhesive used on the copper tape to connect the segments of the sensor. Preliminary tests showed, however, that the remaining three sensors were in good condition and exhibited good performance with little spillover between sensors (see below).

Characterization of the Open-Loop Model

In this section, the methodology used to characterize parameters of the modal sensors and elastic link dynamics is described. A Hewlett-Packard 3462 Fast Fourier Transform Dynamic Signal Analyzer was used to measure the experimental transfer functions presented herein.

Although an infinite set of modal equations is actually needed to model the forced vibrations of a beam, a finite set can be used to approximate the behavior, as in Eq. (2). Keeping the first n modes, we can write

$$\ddot{x}(t) = Ax(t) + BT_e(t) \tag{8}$$

where $x(t)$ is the vector of modal coordinates $q_i(t)$ and $\dot{q}_i(t)$, and the matrices A and B are given by

$$A = \begin{bmatrix} 0 & 1 & & & & & \\ 0 & -a_h & & & & 0 & \\ & & 0 & 1 & & & \\ & & -\omega_1^2 & -2\zeta_1\omega_1 & & & \\ & & & & \ddots & & \\ & 0 & & & & 0 & 1 \\ & & & & & -\omega_n^2 & -2\zeta_n\omega_n \end{bmatrix}$$

$$B = \frac{1}{I_{et}} \begin{bmatrix} 0 \\ 1 \\ 0 \\ \phi_1'(0) \\ \vdots \\ 0 \\ \phi_n'(0) \end{bmatrix}; \quad x(t) = \begin{bmatrix} q_0(t) \\ \dot{q}_0(t) \\ q_1(t) \\ \dot{q}_1(t) \\ \vdots \\ q_n(t) \\ \dot{q}_n(t) \end{bmatrix} \tag{9}$$

All identification tests were done with the shoulder actuator locked and the air supply for the elbow air pad shut down. The identified frequencies are summarized in Table 3.

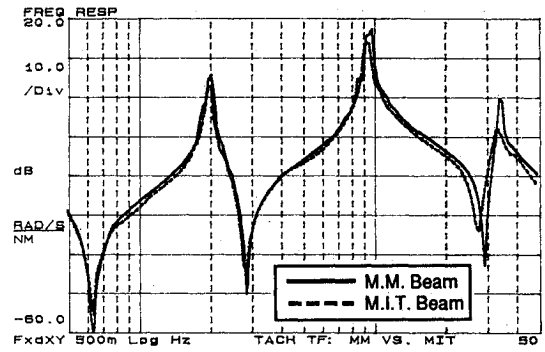

Fig. 4 Transfer function from elbow torque to elbow angular rate for Martin Marietta and MIT beams.

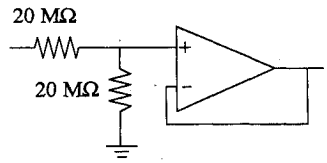

Fig. 5 Impedance buffer circuit.

Elbow Joint Modal Slope Coefficients

The general expression for the transfer function $H_{col}(s)$ from motor torque T_E to motor angular velocity $\dot{\theta}_E(t)$ is

$$H_{col}(s) = \frac{1}{I_{et}s + B} \prod_{i=1}^{n} \frac{(s/\Omega_i)^2 + 2\zeta_{\Omega_i}(s/\Omega_i) + 1}{(s/\omega_i)^2 + 2\zeta_{\omega_i}(s/\omega_i) + 1} \tag{10}$$

where H_{col} is characterized by an alternating set of n lightly damped zeros and poles, as shown in Fig. 4. A least-squares curve fit was used to identify the frequencies Ω_i and ω_i and their damping coefficients ζ_{Ω_i} and ζ_{ω_i}.

The unknown modal slopes $\phi_i'(0)$ were computed by equating $H_{col}(s)$ to the residue expansion derived from the system state equations, Eqs. (8) and (9). The residue expansion for the same open-loop transfer function is

$$H_{col}(s) = \frac{1}{I_{et}s + B} + \frac{1}{I_{et}} \sum_{i=1}^{n} \frac{[\phi_i'(0)]^2 s}{s^2 + 2\zeta_{\omega_i}\omega_i s + \omega_i^2} \tag{11}$$

Therefore, once the n frequencies ω_i and Ω_i are known, we can readily compute the modal slopes $\phi_i'(0)$ by equating the two truncated expressions, Eqs. (10) and (11).

Modal Sensor Output Gains

In an open-circuit configuration, the capacitance of the PVDF and the developed charge result in a potential difference across the electrodes. Direct input into a typical laboratory instrument with 1 MΩ input impedance introduces a first-order high pass filter with 1/RC corner frequency, where R is the input impedance of the instrument and C is the sum of the film's capacitance and the instrument's input capacitance. For these sensors, that corner frequency was approximately 5 Hz. Two approaches exist for impedance buffering these sensors: low input-impedance "charge amplification" or high input-impedance "voltage amplification." For reasons of perceived simplicity, we chose voltage amplification, employing the circuit of Fig. 5, a voltage follower. This amplifier, together with the piezo film capacitance, has the characteristics of a high pass filter with corner frequency of approximately 0.15 Hz.

With a high-impedance voltage follower, the output of the sensor is a voltage $V = Q/C$, where Q is given by Eq. (1) and the sensor capacitance C is given in Table 2. Using Eq. (2), the

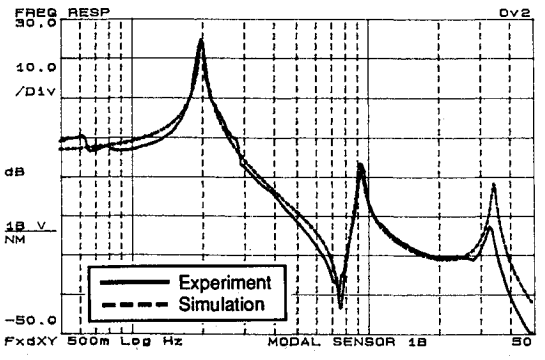

Fig. 6 Transfer function from elbow torque to sensor 1B output.

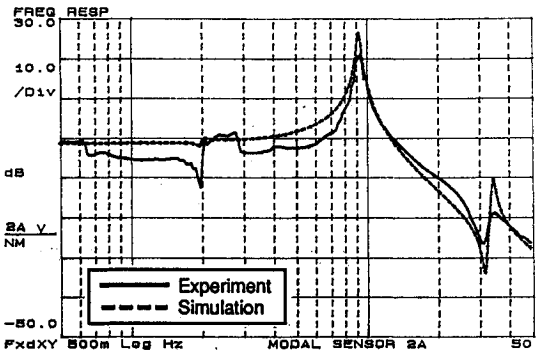

Fig. 7 Transfer function from elbow torque to sensor 2A output.

expression for the output voltage of sensor k in terms of the system modal amplitudes becomes

$$V_k(t) = \sum_{i=1}^{n} C_{ki} q_i(t) \tag{12}$$

where C_{ki} are the (as yet unknown) modal sensor gains. From the modal equations, Eqs. (8) and (9), the elastic coordinates $q_i(t)$ are related to torque T_E by the following Laplace transform:

$$q_i(s) = \frac{1}{I_{et}} \frac{\phi_i'(0)}{s^2 + 2\zeta_{\omega_i}\omega_i s + \omega_i^2} T_E(s) \tag{13}$$

The transfer function H_k from torque T_E to modal sensor output V_k can be expressed in the pole-residue form using Eqs. (12) and (13):

$$H_k(s) = \frac{1}{I_{et}} \sum_{i=1}^{n} \frac{C_{ki}\phi_i'(0)}{s^2 + 2\zeta_{\omega_i}\omega_i s + \omega_i^2} \tag{14}$$

If the excitation frequency ω is close to a lightly damped resonant frequency ω_i, then from Eqs. (10) and (14) we have the following approximations for the steady-state peak-to-peak amplitudes of hub angular velocity $\dot{\theta}_E(t)$ and modal sensor output V_k:

$$\dot{\theta}_E(j\omega) \simeq \frac{1}{I_{et}} \frac{[\phi_i'(0)]^2}{2\zeta_{\omega_i}\omega_i} T_E(j\omega) \tag{15}$$

$$V_k(j\omega) \simeq \frac{1}{I_{et}} \frac{C_{ki}\phi_i'(0)}{2\zeta_{\omega_i}\omega_i^2} T_E(j\omega) \tag{16}$$

Table 4 Experimental sensor gains

	C_{ki}		
	Sensor		
Mode no.	1B	2B	2A
1	264	−3.75	−3.21
2	36.3	−1390	1250
3	−344	−425	284

The ratio of V_k to $\dot{\theta}_E(t)$ was measured experimentally at each resonant frequency ω_i. The unknown modal sensor gains were obtained from Eqs. (15) and (16):

$$C_{ki} = j\omega_i\phi_i'(0)\left[\frac{V_k(j\omega_i)}{\dot{\theta}_E(j\omega_i)}\right]_{\text{meas}} \tag{17}$$

The modal sensors were thus calibrated against the elbow hub tachometer. The sign of the coefficient C_{ki} was determined by observing whether the modal sensor signal was in phase or in opposition of phase with the hub sensor signal. Table 4 shows the measured gains of all sensors. Figures 6 and 7 show the measured open-loop transfer functions for sensors 1B and 2A. Notice that sensor 1B's response to the second mode is about 30 dB lower than its response to the first mode. Similarly, sensor 2A shows little sensitivity to the first and third modes.

Comparison of Martin Marietta and MIT Beams

It was desired to compare the output of the modal sensors with the results of estimators for the flexible states of the system. As is standard practice, the estimators were driven by strain gauge measurements. So as not to damage the full-length modal sensors, the strain gauges were mounted on a second aluminum beam. As shown in the frequency response plots of Fig. 4, the two beams have almost identical dynamic properties (see also Table 3). The higher damping exhibited by the MIT beam in the third mode could be attributed to passive damping introduced by the layers of material associated with the mounting of the sensors.

The strain gauge output gain matrix was identified in a similar manner to that used for the modal sensors. Two strain gauges were mounted on the Martin Marietta (MM) beam: one close to the actuator shaft ($x_1 = 0.127$ m) and one near the middle of the beam ($x_2 = 0.459$ m). The location of strain gauge 1 was chosen based on the analytically predicted mode shapes; the corresponding eighth-order transfer function features an alternating pole-zero pattern, i.e., the strain gauge is "collocated" with the actuator for the first three elastic modes. The location of strain gauge 2 was selected so that, at x_2, the second derivative of the second mode shape was nearly zero (see Fig. 3). Thus, the second mode was almost unobservable from strain gauge 2.

Application to Space Robotics

The modal sensors were designed with the intention of using them in advanced feedback control schemes in lieu of estimates for the flexible states. The scope of the work being presented in this paper, however, is limited to the validation of the modal sensors through comparison of measured modal amplitudes with those predicted both by simulation and by the use of an estimator. An alternative viewpoint is that the modal sensors permit validation of estimators.

In this section we present two experiments with associated simulations and estimators. For the first experiment, the shoulder joint of the manipulator was clamped, and the air supply for the elbow air pad was shut down. This resulted in a kinematically linear one-link flexible manipulator. In the second experiment, the entire manipulator in the rigid-flexible configuration with the shoulder joint free to move was used.

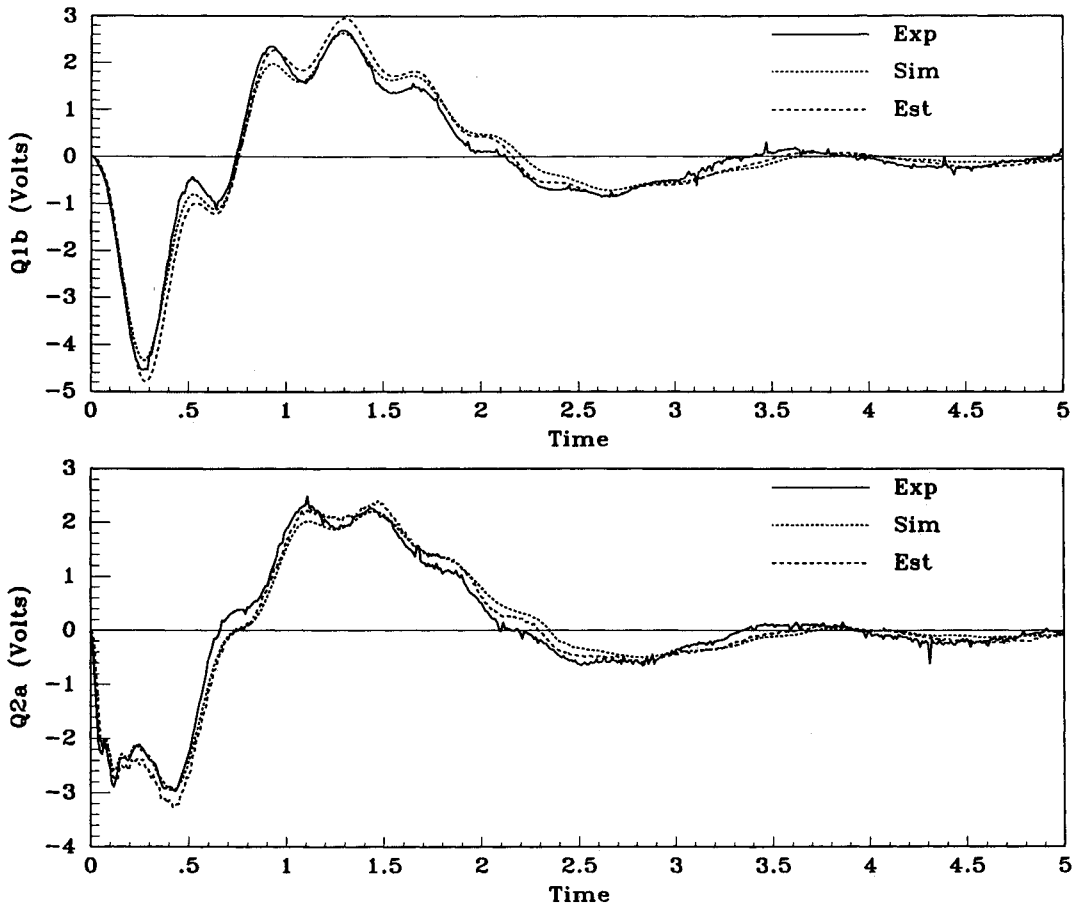

Fig. 8 Comparison of modal sensor outputs, linear estimator outputs, and simulation results for the one-link experiment.

In both cases, reference angle step commands were input at the joints through collocated proportional-derivative (PD) controllers. The output of the modal sensors was then compared to simulation results and estimator outputs. For the two-link case, several estimator designs with varying degrees of simplification of the nonlinear equations of motion were compared.

In the following, because of the significant effect of the sensor high-pass dynamics, we compare sensor outputs rather than modal amplitudes. The process of filtering the simulation and estimator flexible states (modal amplitudes) to obtain simulated sensor outputs turned out to be numerically more robust than trying to filter the sensor output signals (off line) and then "inverting" the sensor output matrix to obtain experimental modal amplitudes. As suggested earlier, direct measurement of the modal amplitudes almost down to dc could be obtained by increasing the input impedance of the voltage amplification impedance buffer. Since higher impedance renders the signal more susceptible to noise, and the LSM testbed is a high electromagnetic interference (EMI) environment, shielding issues may be important.

One-Link Case

The shoulder joint was clamped and the air supply to the elbow air pad was shut down for this experiment. With a low bandwidth (about 0.3 Hz) discrete collocated filtered PD controller running at 100 Hz sampling rate,[11] a 30-deg step input was commanded at the elbow joint. Outputs from the modal sensors as well as from the resolver and tachometer were recorded, and the experiment was then repeated for the beam with the strain gauges. Figure 8 shows the outputs of modal sensors 1B and 2A together with estimator outputs and simulation results. Sensors 2A and 2B had nearly identical responses.

The estimator, a fourth-order linear quadratic estimator (LQE), was implemented discretely at 100 Hz off line using only the measurements from the two strain gauges. Only the first two flexible modes were kept in the estimator model (no rigid body dynamics). Because the estimator was based on the same model as the simulation, it was a perfect estimator of the flexible states as far as the simulation was concerned. This accounts for the very close agreement between the simulation and the estimator results.

It is clear from Fig. 8 that there is excellent agreement between all three forms of sensor outputs (about 10–15% maximum amplitude error). It is noteworthy that the sensor signal exhibits a large voltage level for moderate tip deflections (approximately 5 cm) and is clean (large signal-to-noise ratio) even in the presence of large EMI due to noise from the PWM amplifiers driving the joint motors.

Two-Link Case

For the two-link experiment, independent discrete joint PD controllers, again at a sampling rate of 100 Hz, were implemented. These had bandwidths of 0.7 and 0.27 Hz for the shoulder and elbow controllers, respectively. This time, reference command angle steps of -20 and -40 deg were input at the shoulder and elbow joints, respectively. The initial relative elbow angle was 90 deg. As in the one-link case, the experiment was performed twice: once for the beam with the modal sensors, and once for the beam with the strain gauges. Figure 9 shows the outputs of modal sensors 1B and 2A together with simulation results and estimator outputs.

Several nonlinear estimators, as well as a linear estimator, were designed and compared for this kinematically and dynamically nonlinear case. First of all, the system dynamics

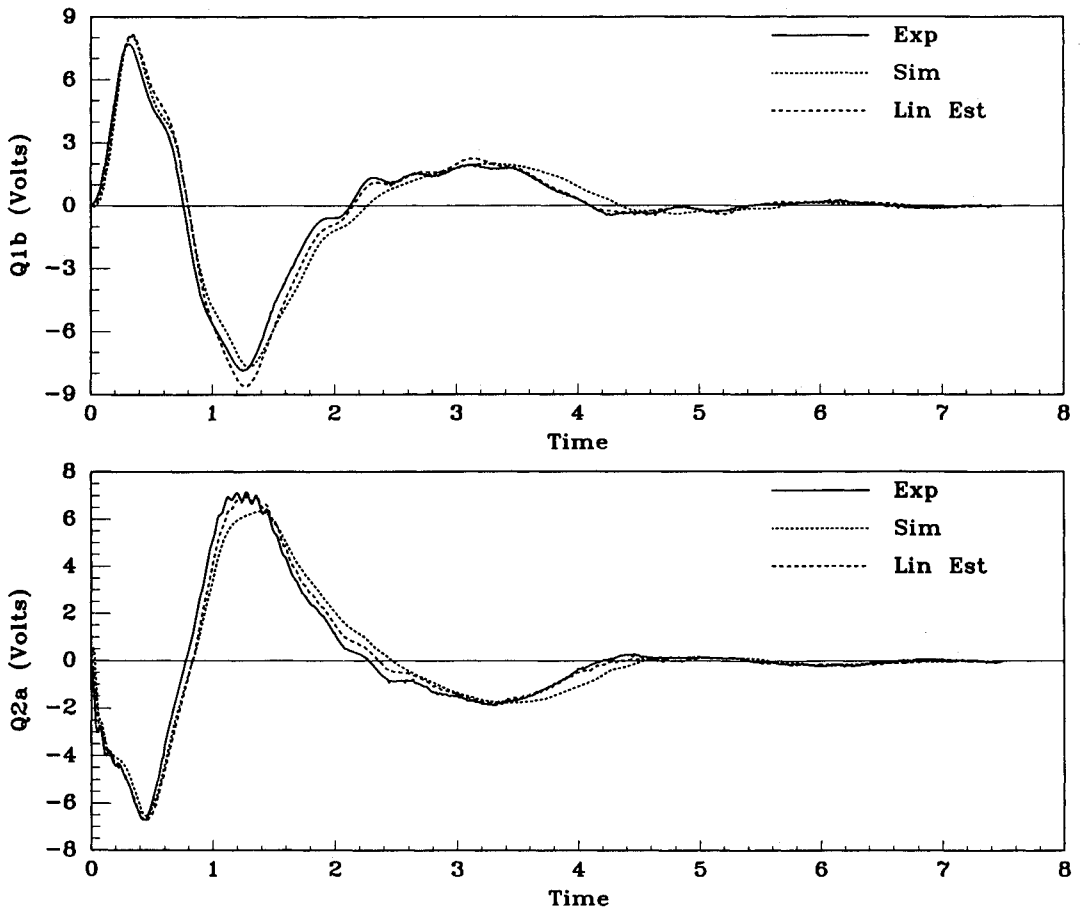

Fig. 9 Comparison of modal sensor outputs, linear estimator outputs, and simulation results for the two-link experiment.

were linearized about a nominal rigid-body configuration determined by a relative elbow angle of 70 deg and by zero angular rates. Using this linear model, an LQE design was effected using measurements from two strain gauges and from the shoulder and elbow resolvers. The constant estimator gains so obtained were then used in four different estimators that were implemented off line. The first three estimators consisted of the nonlinear plant dynamics in varying degrees of simplification[15]: the exact equations of motion to first order in small generalized elastic coordinates and rates (the consistent equations); the "ruthlessly linearized" equations of motion, in which all nonlinear terms containing the elastic states are ignored (including those in the mass matrix); and finally a rate-linear system of equations that still preserved the mass matrix dependency on configuration.

Surprisingly, all three of the aforementioned estimators yielded very similar results, the error being on the order of the width of the plotting line. The linear estimator, in which the linear design plant dynamics were used to estimate the flexible states of the nonlinear plant, also yielded very good results (about 10% maximum error from the simulation) as shown in Fig. 9. Only the linear estimator (the worst case) is shown in Fig. 9 since the nonlinear estimators' results were much closer to the simulation results and nearly overplotted.

The close agreement between the results from the three nonlinear estimators could be due to the "mild" nature of the commanded slew. The maximum angular rates achieved in this maneuver were under 0.1 and 0.15 Hz for the shoulder and elbow, respectively. This is well below the first bending frequency of the outer link and indicates that little difference is to be expected between the simplified models and the consistent dynamic models (see Ref. 15). For much larger elbow relative angle excursions at greater angular rates (closer to the fundamental bending frequency of the outer link), the discrepancies could be more noticeable. More work needs to be done in this area.

Conclusions

Modal sensors yield large, clean signals and have easily characterized dynamics. Increasing the amplifier input impedance will yield the modal amplitudes directly, while properly shielding the sensor and amplification electronics will further reduce noise-related problems. Modal sensors perform at least as well as typical estimators for the flexible states without the computational overhead associated with estimators. In other words, they present the possibility of full-state feedback. For "limited angle" stop-stop slew maneuvers, it seems that even the simplest of estimators yields very good results.

Acknowledgments

This research was supported by Martin Marietta Astronautics Internal Research and Development funds and by the Air Force Office of Scientific Research under Grant AFOSR-88-0029B.

References

[1]Öz, H., and Meirovitch, L., "Stochastic Independent Modal-Space Control of Distributed Parameter Systems," *Journal of Optimization Theory and Applications,* Vol. 40, No. 1, 1983, pp. 121-154.

[2]Meirovitch, L., and Baruh, H., "The Implementation of Modal Filters for Control of Structures," *Journal of Guidance, Control, and Dynamics,* Vol. 8, No. 6, 1985, pp. 707-716.

[3]Miller, S. E., and Hubbard, J., "Theoretical and Experimental Analysis of Spatially Distributed Sensors on a Bernoulli-Euler Beam," Charles Stark Draper Laboratory, CSDL-C-5953, Cambridge, MA, July 1987, p. 11.

[4]Lee, C.-K., and Moon, F. C., "Modal Sensors/Actuators," *Journal of Applied Mechanics,* Vol. 57, No. 2, 1990, pp. 434–441.

[5]Notestine, R. J., and Beninato, J. M., "Piezoelectric Film as a Distributed Vibrational Mode Sensor," Experimental Projects Course Final Rept., Massachusetts Inst. of Technology, Cambridge, MA, Dec. 1988.

[6]Crawley, E. F., and de Luis, J., "Experimental Verification of Distributed Piezoelectric Actuators for Use in Precision Space Structures," *Proceedings of the 27th AIAA/ASME/ASCE/AHS Structures, Structural Dynamics, and Materials Conference,* AIAA, New York, 1986, Pt. 1, pp. 116–124.

[7]Bailey, T., and Hubbard, J. E., Jr., "Distributed Piezoelectric-Polymer Active Vibration Control of a Cantilever Beam," *Journal of Guidance, Control, and Dynamics,* Vol. 8, No. 5, 1985, pp. 605–611.

[8]Tzou, H. S., "Integrated Sensing and Adaptive Vibration Suppression of Distributed Systems," *Recent Advances in Control of Nonlinear and Distributed Parameter Systems, Robust Control, and Aerospace Control Applications,* edited by J. Bentsman and S. M. Joshi, ASME-DSC-Vol. 10, ASME, New York, 1988, pp. 51–58.

[9]Meirovitch, L., *Analytical Methods in Vibrations,* Macmillan, New York, 1967, pp. 141–143.

[10]Blevins, R. D., *Formulas for Natural Frequency and Mode Shape,* Robert E. Krieger Publishing, Malabar, FL, 1979, pp. 107–134.

[11]Schmitz, E., "Modelling and Control of a Planar Manipulator with an Elastic Forearm," *Proceedings of the 1989 IEEE Conference on Robotics and Automation,* Vol. 2, IEEE Computer Society Press, Washington, DC, 1989, pp. 894–899.

[12]Love, A. E. H., *A Treatise on the Mathematical Theory of Elasticity,* 4th ed., Cambridge Univ. Press, Cambridge, England, UK, 1927, pp. 463–465.

[13]*KYNAR Piezo Film Technical Manual,* Pennwalt Corp., Valley Forge, PA, 1987, p. 50.

[14]Collins, S. A., Miller, D. W., and von Flotow, A. H., "Sensors for Structural Control Applications Using Piezoelectric Polymer Film," MIT Space Engineering Research Center, SERC #12-90, Cambridge, MA, Oct. 1990, pp. 32–41.

[15]Padilla, C. E., "Nonlinear Strain-Displacement Relations in the Dynamics of a Two-Link Flexible Manipulator," S.M. Thesis, Dept. of Aeronautics and Astronautics, Massachusetts Inst. of Technology, Cambridge, MA, May 1989, pp. 36–46.